Temperature Elevation in an Instrumented Phantom Insonated by B-Mode Imaging, Pulse Doppler and Shear Wave Elastography

Maha Issaoui, Piero Miloro, Xavier Balandraud, Ian Rivens, Michel Grédiac, Benoît Blaysat, Lemlih × Ouchchane, Amélie Delabaere, Marie-Pierre Sauvant-Rochat, Didier Lemery

Temperature elevation in an instrumented phantom insonated by B-mode imaging, Pulse-Doppler and Shear Wave Elastography

Maha Issaoui[1], Piero Miloro[2], Xavier Balandraud[1], Ian Rivens[3], Michel Grédiac[1], Benoit Blaysat[1], Lemlih Ouchchane[4,5], Amélie Delabaere[4,6], Marie-Pierre Sauvant-Rochat[1,7], and Didier Lemery[4,6]

[1] Université Clermont Auvergne, CNRS, SIGMA Clermont, Institut Pascal, F-63000 Clermont-Ferrand, France
[2] Ultrasound and Underwater Acoustics, National Physical Laboratory, Teddington, TW11 0LW, UK
[3] Department of Physics at The Institute of Cancer Research and The Royal Marsden NHS Foundation Trust, London, United Kingdom
[4] Université Clermont Auvergne, CHU Clermont-Ferrand, CNRS, SIGMA Clermont, Institut Pascal, F-63000 Clermont-Ferrand, France
[5]Département de Santé Publique, Unité de Biostatistique et Informatique Médicale, CHU de Clermont-Ferrand, F-63000 Clermont-Ferrand, France
[6] Pôle Femme et Enfant, CHU de Clermont-Ferrand, F-63000 Clermont-Ferrand, France
[7] Département de Santé Publique et Environnement, Université Clermont-Auvergne, UFR Pharmacie, F-63000 Clermont-Ferrand, France

Address correspondence to: Maha Issaoui, Institut Pascal, Campus Universitaire des Cézeaux, 4 avenue Blaise Pascal, F-63178 Aubière, France. E-mail: maha.issaoui@uca.fr, issaouimaha@hotmail.fr

Abstract — Diagnostic ultrasound is the gold standard for obstetric scanning and one of the most important imaging techniques for perinatal and neonatal monitoring and diagnosis. Ultrasound provides detailed real-time anatomical information, including blood flow measurements and tissue elasticity. The latter is provided through various techniques including Shear Wave Elastography (SWE). SWE is increasingly used in many areas of medicine, especially in detection and diagnosis of breast, thyroid, and prostate cancers and liver disease. More recently, SWE has found application in gynaecology and obstetrics. This method mimics manual palpation, showing the elastic properties of soft biological tissues. Despite its rising potential and expanding clinical interest in obstetrics and gynaecology (such as for assessment of cervical ripening or organ development and structure during pregnancy), its effects on and potential risks to the developing fetus remain unknown. Risks should be evaluated before recommendations are made on the use of SWE by regulatory bodies. Because ultrasound is known to produce thermal and mechanical effects, this study measured the temperature increase caused by B-mode, Pulse-Doppler (PD) and SWE, using an instrumented phantom with eleven embedded thermocouples. Experiments were performed with an Aixplorer® diagnostic ultrasound system (Supersonic Imagine, Aix-en-Provence, France). As expected, the largest heating was detected by the thermocouple closest to the surface in contact with the transducer (2.9°C for SWE, 1.2°C for PD, 0.7°C for B-mode after 380-second excitation). Both conduction from the transducer face and direct heating due to ultrasound waves contribute to temperature increase in the phantom with SWE showing a larger temperature increase than PD and B-mode. This manuscript offers a methodological approach and reference data for future safety studies, as well as initial recommendations about SWE safety in obstetrics and gynaecology.

Keywords: Shear wave elastography; Ultrasound safety; Phantom; Thermocouple; Temperature change; tissue mimic; thermal damage; Obstetrics; Gynaecology; Fetus

INTRODUCTION

Shear wave elastography (SWE) is a non-invasive diagnostic imaging technique used for mapping the elastic properties of tissues (Parker et al. 2011). This modality is being increasingly used in many areas of medicine, offering high-quality diagnostic examination, as it increases specificity and improves diagnostic accuracy, as discussed below. SWE provides the elastic properties of soft biological tissues, from the measurement of the speed of propagation of ultrasound radiation induced shear waves. Ophir et al. developed a strain-measuring compression elastography method (Ophir et al. 1991). Elastography was initially developed by Wilson and Robinson (1982) with the aim of quantifying Young's modulus for diagnostic purposes. Young's modulus quantifies the stiffness, defined as stress divided by strain, of a solid material. Tissue elasticity can be explored either by studying its deformation under the effect of constant pressure (*i.e.* the static method) or by studying the propagation of a mechanical shear wave induced by an oscillating source (*i.e.* the dynamic method) (Dickinson and Hill 1982). SWE represents an ultrasound-based approach to manual palpation medical examination (Fink 2013). Modern scanners like that used in this study generate the shear wave by producing a displacement in the tissue through a focused, high intensity and short duration ultrasonic push.

SWE has already been demonstrated that elastography is useful for characterizing malignant tumours in breast (Klotz et al. 2014), thyroid (Monpeyssen et al. 2013) and prostate (Dudea et al. 2011), as well as lymph nodes structure (Alam et al. 2008), and localized (Menten et al. 2010; Sandulescu et al. 2012) or diffuse liver diseases (Kennedy et al. 2018).

The use of SWE has recently been extended to gynaecology diagnosis of uterine disorders (Metin et al. 2016; Stoelinga et al. 2014; Thomas et al. 2007) and to obstetrics (Ogawa et al. 2012) for cervix stiffness/ripening assessment (Duan et al. 2020; Egorov et al. 2020; Hernandez-Andrade et al. 2013; Pereira et al. 2014). Potential indications of SWE in fetal and uterine imaging during pregnancy include placental examination (Akbas et al. 2019; Kılıç et al. 2015; Cimsit et al. 2015) and fetal organ development and structure. In fact, SWE has recently been explored to assess fetal brain (Diguisto et al. 2017), lung (Mottet et al. 2019) and liver (Zheng et al. 2016), outside regulatory indication scopes. In obstetrics, the first use of this ultrasound technique was for the study of cervix (maturation, threats of premature delivery). The measurement techniques involving direct application of deformation (the only ones used until now) are not perfect, especially in terms of reproducibility. Histological modifications of the placenta in certain pathologies of pregnancy (*i.e.* pre-eclampsia) could have an observable effect in terms of tissue elasticity. In the same way, the evolution linked to the maturation of certain organs could also be of clinical interest. The examination of the fetal lungs (in particular in order to assess their spontaneous maturity or after preventive treatment of hyaline membrane disease by corticosteroid therapy) and the pre-implantation endometrium in assisted reproductive technology (ART) are typical examples. Few researchers have addressed the teratogenic effects of fetal elastography, one example was the discussion held between K. Preisand and G. Rus at the World Congress of Fetal Medicine in 2016 (Massó et al. 2017): although no apparent histological changes following ultrasound elastography have been reported, the absence all bioeffects could not be excluded (Sugitani et al. 2013). One of the first studies using SWE to assess cervical ripening in 2012 (Peralta et al. 2017), conducted in the lack of any regulatory framework, was the subject of comments (Massó et al. 2017) highlighting the need for follow-up of children exposed *in utero*. The potential teratogenic effects of elastography were subsequently

explored by a follow-up study of the children at 4 years of age, focusing on the results of a neonatal hypoacusis screening test and medical records. The exposed population was compared to the reference population using a contingency-table analysis to assess excess risk. Hypoacusis was reported in a late premature case (36 weeks, 1860 g), and was attributable to a Prader–Willi-like phenotype. No other case negative outcomes were observed, though a larger sample size would be beneficial. Some *in vivo* experiments have also shown that the threshold temperature increase for teratogenic effects induced by hyperthermia is estimated at 1.5°C for an exposure of 5 min (Abramowicz et al. 2008).

Considering the increasing number of publications on elastography, the World Federation for Ultrasound in Medicine and Biology (WFUMB) first published guidelines for its clinical use in August 2011. The initial consensus meeting was held in March 2013 and led to the development of general guidelines for elastography (Shiina et al. 2015), and specifically for imaging of breast (Barr et al. 2015), liver (Ferraioli et al. 2015), prostate (Barr et al. 2017) and thyroid (Cosgrove et al. 2017). These guidelines did not distinguish between the different elastography modes. The European Federation of Societies for Ultrasound in Medicine and Biology (EFSUMB) later published guidelines and recommendations for the clinical use of ultrasound elastography (Dietrich et al. 2017; Săftoiu et al. 2018). Neither updated recommendation included obstetric application. The only British Medical Ultrasound Society (BMUS) recommendations regarding obstetrics focus on the use of B-mode and Pulse-Doppler (PD) imaging (BMUS Safety Group 2010). To date, SWE has not been approved by the Food and Drug Administration (FDA) for clinical applications in obstetrics.

Ultrasound can lead to two main types of potentially damaging effects on biological tissues, namely thermal and mechanical effects (Shankar and Pagel 2011). A developing fetus could be particularly sensitive to the aforementioned effects (Issaoui et al. 2018).

Previous studies have measured the temperature increase due to ultrasonic push used in SWE (Lui et al. 2014). A pre-clinic experimental approach is also required, and developing experimental techniques to measure the temperature rise in biological tissue caused by ultrasound is of great interest for a variety of diagnostic and therapeutic applications.

Previous (non-SWE) studies have been performed to assess whether the temperature increase in soft tissue mimicking materials can exceed the aforementioned safety limits (Miloro et al. 2017; Calvert et al. 2007; Clarke and terHaar 1997; Palmeri and Nightingale 2004; Skurczynski et al. 2009). Thermocouples are known to generate artifacts (Morris et al. 2008), the main source being the viscous heating. In the work, mitigating actions have been taken to reduce the artifacts. Different techniques that involve the analysis of ultrasound images have been developed (Alvarenga et al. 2017), but require a high level access to the raw data of the ultrasound scanners.

The present study aims to compare SWE imaging with two diagnostic imaging modes which are in routine clinical use for scanning of pregnant women (B-mode and pulsed Doppler (PD)). For this purpose, heating patterns caused by the three modalities were characterized in an instrumented phantom, composed of a well characterized Tissue Mimicking Material (TMM) with 11 embedded fine-wire thermocouples. It is important to note that a perspective of the study concerns the health risk of SWE for fetus in terms of temperature rises. The experimental program was carried out with a view to assessing health risks in order to meet a clinical objective in obstetrics in the future.

MATERIALS AND METHODS

Instrumented Phantom

An acousto-thermal phantom with embedded thermocouples was designed, manufactured and used to measure the temperature increase due to diagnostic ultrasound excitation. The phantom was developed at the National Physical Laboratory (NPL, Teddington, UK). The tissue mimicking material (TMM) used in the phantom was the agar-based gel described in the IEC 60601-2-37 (2007). The recipe, based on 3% w/w of agar, includes glycerol to match the speed of sound of soft tissues, as well as additives (silicon carbide and aluminium oxide) to adjust the attenuation and backscatter coefficients. A plastic frame mould was 3D-printed at NPL, in order to cast a 136×80×80 mm^3 block of TMM (see Fig. 1-a to 1-c). For use and storage, the phantom was kept in an aqueous solution of 11.9% w/w glycerol in order to prevent dehydratation and glycerol leaching out of the TMM.

The main acoustic properties of the TMM were measured at NPL using the finite amplitude insertion substitution (FAIS) method described by Baêsso et al. (2019): attenuation was almost linear with frequency (0.57±0.05 $dB \cdot cm^{-1} \cdot MHz^{-1}$) and speed of sound was 1540 $m \cdot s^{-1}$ ±1%. Thermal properties, measured using a hand held device (TEMPOS, Meter Group, Pullman, WA, USA), were: specific heat capacity of 3770 $J \cdot kg^{-1} \cdot K^{-1}$, thermal conductivity of 0.58 $W \cdot m^{-1} \cdot K^{-1}$ and thermal diffusivity of 0.15 $mm^2 \cdot s^{-1}$, with a quoted measurement uncertainty of 10%. The density of the TMM was 1070±30 $kg \cdot m^{-3}$ (IEC 60601-2-37, 2007). These values are comparable to those of soft tissues. In particular, the IT'IS Database of Tissue Properties (Hasgall et al. 2018) reports values of 3676 $J \cdot kg^{-1} \cdot K^{-1}$, 0.53 $W \cdot m^{-1} \cdot K^{-1}$ and 1105 $kg \cdot m^{-3}$ for the specific heat capacity, the thermal conductivity and the density of uterine tissues, respectively, while the IEC 60601-2-37 (2007) reports 0.6 $dB \cdot cm^{-1} \cdot MHz^{-1}$ and 1575 $m \cdot s^{-1}$ for acoustic attenuation and speed of sound in soft tissues.

Eleven 75 μm diameter K-type insulated thermocouples from Omega Engineering (5SRTC-TT-KI-40-1 M, Manchester, UK) were embedded into TMM gel at pre-determined positions in the phantom using notches in the frame used to mold the gel. The carefully

designed wire matrix is shown in Fig. 1-d and 1-e. One of the 11 thermocouples (called ref in the figure), was used during the tests as a reference to track environmental thermal fluctuation. It was placed at the location (x = 0 mm, y = 24 mm, z = 74 mm) to be outside the ultrasonic excitation, so that it can be reasonably assumed that it provides the externally affected TMM reference conditions. The present study is based on measuring temperature change due to ultrasound excitation at the locations of the ten other thermocouples whose coordinates are given in Table 1. The position of the thermocouples was chosen based on the results of a previous work (Issaoui et al. 2020) and assuming symmetry in the temperature field with respect to the two symmetry planes of the transducer. To limit the number of thermocouples and reduce the complexity of the instrument, it was decided to place all of them in one quarter of the phantom. Because the imaging probe can be orientated however the user prefers, this does not limit the flexibile use of the phantom. Thermocouples Tc-1 to Tc-7 were designed to be located in the transducer imaging plane (y = 0 mm) with Tc-8*, Tc-9* and Tc-10* outside this plane by either 10 or 13 mm (*: symbol refering to thermocouples located out of the transducer plane).

Experimental setup

Preliminary tests were performed by three operators (MI, PM and IR) at the Institute of Cancer Research, London (ICR) to check the locations and the proper functioning of the TMM embedded thermocouples, and to validate the feasibility of using the instrumented phantom with an Aixplorer® scanner. Subsequently, the core of the study was carried out at the department of obstetrics and gynaecology of the University Hospital of Clermont-Ferrand (CHU), France. The test campaign was performed by five operators (MI, XB, BB, MG, DL). The echography system used was an Aixplorer® (Supersonic Imagine, Aix-en-Provence, France), featuring B-mode, PD and SWE imaging modes. Only a curved

199 SC6-1 probe (Supersonic Imagine, Aix-en-Provence, France) featuring 192 piezoelectric
200 elements and a bandwidth of 1–6 MHz, typically used in obstetrics, was employed. The
201 transducer face has a thickness of 15 mm, a radius of curvature of 100 mm and a frontal area
202 of 73×15 mm^2. The imaging transducer was clamped in placed in contact with the top surface
203 of the phantom as shown in Fig. 2-a. Acoustic gel was employed to couple the phantom to the
204 transducer. Figure 2-b shows a typical B-mode image of the thermocouple wires. Table 2
205 provides the ultrasound settings used for each of the three imaging modes. For each of them,
206 the "obstetric preset" option was chosen, and no other settings were changed during the tests.
207 Ultrasonic imaging exposures lasted 380 seconds. This is a typical duration of an obstetric B-
208 mode examination (Martin et al. 2015). Although not directly comparable to a clinical
209 scenario, for comparison purposes, it was decided to consider the same duration for all the
210 three modalities. Temperature measurements began twenty seconds before exposure and
211 lasted 30 min so that the return to thermal equilibrium could be monitored. Temperature data
212 from the thermocouples were recorded using a TC08 datalogger (PicoTech, St Neots, UK)
213 connected to a computer. Recording frequency was set to 1 Hz. The standard deviation of the
214 noise in temperature measurements was lower than 0.01°C (measurable for instance during
215 the first 20 seconds before ultrasound excitation in Fig. 3). Ultrasound induced temperature
216 changes were calculated by subtracting the reference thermocouple temperature to the value
217 of thermocouples Tc-1 to Tc-10* at every time. The variation of the temperature reading for
218 the reference thermocouple was always below 0.05°C during the 400 s of insonation.
219

RESULTS

Figure 3 presents the temperature change measured by the ten thermocouples as a function of time for (a) B-mode, (b) Pulse-Doppler (PD) and (c) Shear Wave Elastography (SWE). The first vertical dashed line indicates ultrasound activation, at time t = 20 s. The second one corresponds to the end of exposure, at t = 400 s. Values are shown until t = 750 s in order to demonstrate initial cooling. Temperature increases at t = 400 s are shown in Figure 4 using circles with diameters proportional to the maximum temperature change measured for each mode, which always occurs for Tc-1). This representation gives a better visualization of the temperature distributions for each mode but does not allow comparison between imaging modes. Finally, Figure 5 compares the temporal temperature variations of the three thermocouples closest to the transducer (Tc-1, Tc-10* and Tc-7) for the three imaging modes. Some important features can be extrapolated from the graphs:

- the maximum temperature increase was about 0.7°C, 1.2°C and 2.9°C for B-mode, PD and SWE respectively. After validation of the device and numerous preliminary tests, experiments were repeated twice and good reproducibility of the results was observed for each ultrasound mode (the maximum temperature variations between repeats was measured to be lower than 0.1°C for all thermocouples). It is worth noting that the objective of the study was not to perform a statistical analysis of the results, but to compare three ultrasound modalities among which two are already in routine clinical use for scanning of pregnant women;
- as expected from previous works (Miloro et al. 2017; Issaoui et al. 2020), the highest temperature rises were observed for Tc-1, which was just under the transducer. Large temperature changes were also observed for Tc-10* (more than 50% of the peak

244 increase), which was superficially close to the transducer (4 mm below Tc-1) but
245 10 mm away in the out of plane direction (see Fig. 1-d and 1-e);
246 • The temperature change at Tc-3 is smaller than the temperature change at Tc-2 and
247 Tc-4, whatever the mode under consideration. In particular, Tc-4 readings at 400 s
248 were about 0.04°C, 0.2°C and 0.4°C for B-mode, PD and SWE respectively;
249 • heating was also clearly detected out of the transducer plane for PD and SWE (see Tc-
250 8* to Tc-10*).
251
252 # DISCUSSION
253
254 An instrumented phantom was developed for the assessment of the temperature increase
255 during B-mode, PD and SWE ultrasound imaging. 10 thermocouples were used, and their
256 positioning was not limited to being on the transducer axis. To our best knowledge, the
257 present study is the first one to measure heating variations due to SWE with thermocouples
258 inside a phantom. As expected from previous studies, the largest temperature rises were
259 observed for the thermocouple which was just under the transducer. This is likely to be due to
260 the self heating of the transducer and the effects are visibile also for thermocouples outside
261 the imaging plane (Tc-10). More in depth, direct absorption of ultrasound energy is expected
262 to play a more significant role. The role of absorption is highlighted on the results by an
263 immediate and measurable temperature rise from Tc-2 and Tc-7, more evident in SWE where
264 a higher signal-to-noise ratio was achieved. Due to the proximity of these thermocouples to
265 the transducer, heat transfer is likely to play a role in the temperature readings at the end of
266 the insonation.
267 Furthermore, the temperature increase for Tc-4 was higher than the one observed for
268 Tc-3 (which is closed to the transducer) for all the imaging modes. It is interesting to observe

269 that in SWE mode, Tc-4 is within the focus of the acoustic beam used for generation of the
270 shear waves. Similar observations were made on a sample without embedded thermocouples
271 using surface infrared thermography (Issaoui et al. 2020).

272 Future studies could advantageously couple embedded thermocouples and surface
273 thermographic measurements in order to reconstruct the three-dimensional thermal field in the
274 sample.

275 A limitation of our study is that it was performed on a phantom composed of soft
276 tissue mimicking material only. The BMUS guidelines for the safe use of diagnostic
277 ultrasound equipment (BMUS Safety Group 2010) suggests using the bone thermal index for
278 obstetric scans after the 10^{th} week. Many other studies have shown that heating of bones is
279 much higher than that of soft tissues (Tabaru et al. 2012; Nitta et al. 2001). Further studies
280 should be performed on phantoms containing soft tissues and bone mimicking materials.

281 On the other hand, in clinical practice, other factors such as the almost continuous
282 movement of the transducer, freezing of the output and reviewing acquired data during the
283 examination, blood perfusion and the presence amniotic fluid could reduce the temperature
284 changes deeper in the tissue. The TMM used in the present study was selected to mimic the
285 average acoustic and thermal properties of soft tissues. However, real tissues are
286 inhomogeneous.

287 Thermocouples have been used in the past to measure temperature increases in tissue
288 mimicking materials despite well-known artifacts in the measurements, the most relevant
289 being the viscous heating. Precaution have been taken to minimize these artifacts. The
290 sensitive element of the selected thermocouple was 3.5 times be smaller than the shortest
291 wavelength (257 µm at 6 MHz), following the indications of the IEC committee (IEC 60601-
292 2-37, 2007). The thermocouples were positioned such that the wires were on a plane
293 perpendicular to the acoustic propagation axis (Suo et al. 2019). Furthermore, diagnostic

imaging modes are characterized by small duty cycles, thus reducing the effects of viscous heating (Morris et al. 2008).

Despite the limitations, a clear trend was observed: temperature rise is faster and higher for SWE than by PD and B-mode, with the last two modes already in use in obstetrics for decades. Altough all the measured values, including MI and TI, fall within the safety guidelines of BMUS, these are in the category of time limits.

The temperature rise due to SWE was the highest: about 2.5 times greater than that due to PD, and more than 4 times greater than that due to B-mode. These results also indicate, consistently with previous works (Miloro et al. 2017) that TI is a poor indicator of the actual temperature rise in tissues. If TI is not displayed, like for B-mode and PD, it indicates values below 0.4. These are at least 4 times lower than the TI indicated for SWE, which is not in agreement with the results of this work.

However, recently released EFSUMB guidelines (Kollman et al. 2019), recommend that Pulsed Doppler ultrasound should not be used routinely in early pregnancy (before the 14^{th} week) and when used driven by a clear clinical motivation, the displayed Thermal Index should be less than or equal to 1.0, and exposure time should be kept as short as possible. BMUS guidelines (BMUS Safety Group 2010) also suggest that Pulsed Doppler should not be used without a risk-benefit analysis (and always monitoring the TI) on the head, brain or spine of any fetus or neonate or the eye of a subject of any age.

Based on the existing guidelines, the results of this work suggest that the risks associated with SWE are higher than those associated with B-mode and PD. More in general, the results raise questions about the health risk associated with obstetric SWE, as well as about the approach to be put in place and the standards to be considered when certifying this technique for obstetrical use.

Acknowledgements

The authors would like to thank Professor Bernard Jacquetin, president of the ADOGA (*Association pour le Développement de l'Obstétrique et de la Gynécologie en Auvergne*), France, for the financial support of this study.

References

Abramowicz JS, Barnett SB, Duck FA, Edmonds PD, Hynynen KH, Ziskin MC. Fetal Thermal Effects of Diagnostic Ultrasound. J Ultras Med 2008;27:541–59.

Akbas M, Koyuncu FM, Artunç-Ulkumen B. Placental elasticity assessment by point shear wave elastography in pregnancies with intrauterine growth restriction. J Perinat Med 2019;47:841–46.

Alam F, Naito K, Horiguchi J, Fukuda H, Tachikake T, Ito K. Accuracy of Sonographic Elastography in the Differential Diagnosis of Enlarged Cervical Lymph Nodes: Comparison with Conventional B-Mode Sonography. Am J Roentgenol 2008;191:604–10.

Alvarenga AV, Wilkens V, Georg O, Costa-Félix RPB. Non-invasive estimation of temperature during physiotherapeutic ultrasound application using the average gray-level content of B-Mode Images: a metrological approach. Ultrasound Med Biol 2017;43:1938–52.

Baêsso RM, Costa-Felix RPB, Miloro P, Zeqiri B. Ultrasonic parameter measurement as a means of assessing the quality of biodiesel production. Fuel 2019;241:155–63.

Barr RG, Nakashima K, Amy D, Cosgrove D, Farrokh A, Schafer F, Bamber JC, Jeffrey C, Castera L, Choi BI, Chou YH, Dietrich CF, Ding H, Ferraioli G, Filice C, Friedrich-Rust M, Hall TJ, Nightingale KR, Palmeri ML, Shiina T, Suzuki S, Sporea I, Wilson S, Kudo M. WFUMB guidelines and recommendations for clinical use of ultrasound elastography: Part 2: Breast. Ultrasound Med Biol 2015;41:1148–60.

Barr RG, Cosgrove D, Brock M, Cantisani V, Correas JM, Postema AW, Salomon G, Tsutsumi M, Xu HX, Dietrich CF. WFUMB Guidelines and Recommendations on the Clinical Use of Ultrasound Elastography: Part 5: Prostate. Ultrasound Med Biol 2017;43:27–48.

British Medical Ultrasound Society, Safety group of the. Guidelines for the safe use of diagnostic ultrasound equipment, 2010. https://doi.org/10.1258/ult.2010.100003.

Calvert J, Duck F, Clift S, Azaime H. Surface heating by transvaginal transducers. Ultrasound Obst Gyn 2007;29:427–32.

Cimsit C, Yoldemir T, Akpinar IN. Shear wave elastography in placental dysfunction: comparison of elasticity values in normal and preeclamptic pregnancies in the second trimester. J Ultras Med 2015;34:151–9.

Clarke RL, terHaar GR. Temperature rise recorded during lesion formation by high-intensity focused ultrasound. Ultrasound Med Biol 1997;23:299–306.

Cosgrove D, Barr R, Bojunga J, Cantisani V, Chammas MC, Dighe M, Vinayak S, Xu JM, Dietrich CF. WFUMB Guidelines and Recommendations on the Clinical Use of Ultrasound Elastography: Part 4. Thyroid. Ultrasound Med Biol 2017;43:4–26.

Dickinson RJ, Hill CR. Measurement of soft tissue motion using correlation between A-scans. Ultrasound Med Biol 1982;8:263–71.

Dietrich CF, Bamber J, Berzigotti A, Bota S, Cantisani V, Castera L, Cosgrove D, Ferraioli G, Friedrich-Rust M, Gilja OH, Goertz RS, Karlas T, de Knegt R, de Ledinghen V, Piscaglia F, Procopet B, Saftoiu A, Sidhu PS, Sporea I, Thiele M. EFSUMB Guidelines and Recommendations on the Clinical Use of Liver Ultrasound Elastography, Ultraschall Med 2017;38:16–47.

Diguisto C, Simon EG, Callé S, Ternifi R, Remeniéras J-P, Hervé P, Herve P, Perrotin F. Ultrasonic elastography exploration of the foetal brain: A case of atypical choroid plexus papilloma. J Obst Gyn 2017;37:525–7.

Duan H; Chaemsaithong P; Ju X; Ho SYS; Sun Q; Tai YY; Leung TY, Poon LC. Shear-wave sonoelastographic assessment of cervix in pregnancy. Acta Obstet Gynecol Scand 2020;doi: 10.1111/aogs.13874

Dudea SM, Giurgiu CR, Dumitriu D, Chiorean A, Ciurea A, Botar-Jid C, Coman I. Value of ultrasound elastography in the diagnosis and management of prostate carcinoma. Med Ultrason 2011;13:45–53.

Egorov V, Rosen T, van Raalte H, Kurtenoks V. Cervical Characterization with Tactile-Ultrasound Probe. Open J Obstet Gynecol 2020;10:85–99.

Ferraioli G, Filice C, Castera L, Choi BI, Sporea I, Wilson SR, Cosgrove D, Dietrich CF, Amy D, Bamber JC, Barr R, Chou YH, Ding H, Farrokh A, Friedrich-Rust M, Hall TJ, Nakashima K, Nightingale KR, Palmeri ML, Schafer F, Shiina T, Suzuki S, Kudo M.

WFUMB Guidelines and Recommendations for Clinical Use of Ultrasound Elastography: Part 3: Liver. Ultrasound Med Biol 2015;41:1161–79.

Fink M. Elastography: a new modality of ultrasound imaging. Diagn Interv Imag 2013;94:485.

Hasgall PA, Di Gennaro F, Baumgartner C, Neufeld E, Lloyd B, Gosselin MC, Payne D, Klingenböck A, Kuster N. IT'IS Database for thermal and electromagnetic parameters of biological tissues, Version 4.0, May 15, 2018. DOI: 10.13099/VIP21000-04-0

Hernandez-Andrade E, Hassan SS, Ahn H, Korzeniewski SJ, Yeo L, Chaiworapongsa T, Romero R. Evaluation of cervical stiffness during pregnancy using semiquantitative ultrasound elastography. Ultrasound Obst Gyn 2013;41:152–61.

Issaoui M, Debost-Legrand A, Skerl K, Chauveau B, Magnin B, Delabaere A, Boyer L, Sauvant-Rochat MP, Lemery D. Shear wave elastography safety in fetus: A quantitative health risk assessment. Diagn Interv Imag 2018;99:519–24.

Issaoui M, Balandraud X, Grédiac M, Blaysat B, Ouchchane L,Sauvant-Rochat M-P, Delabaere A,Lemery D. Temperature rise caused by Shear Wave Elastography Pulse-Doppler and B-mode in biological tissue: an infrared thermographic approach. Ultrasound Med Biol 2020;46:325–35.

IEC (International Electrotechnical Commission). IEC 60601-2-37 Medical electrical equipment - particular requirements for the safety of ultrasonic medical diagnostic and monitoring equipment. Geneva: IEC, 2007.

Kennedy P, Wagner M, Castéra L, Hong CW, Johnson CL, Sirlin CB, Taouli B. Quantitative Elastography Methods in Liver Disease: Current Evidence and Future Directions. Radiology 2018;286:738–63.

Killingback AL, Newey VR, El-Brawany MA. Development of a thermal test object for the measurement of ultrasound intracavity transducer self-heating. Ultrasound Med Biol 2008; 34: 2035–42.

Kılıç F, Kayadibi Y, Yüksel MA, Adaletli İ, Ustabaşıoğlu FE, Öncül M, Madazli R, Yilmaz MH, Mihmanli I, Kantarci F. Shear wave elastography of placenta: in vivo quantitation of placental elasticity in preeclampsia. Diagn Interv Radiol 2015;21:202–7.

Klotz T, Boussion V, Kwiatkowski F, Dieu-de Fraissinette V, Bailly-Glatre A, Lemery S, Boyer L. Shear wave elastography contribution in ultrasound diagnosis management of breast lesions. Diagn Interv Radiol 2014;95:813–24.

Kollmann C, Jenderka KV, Moran C M, Draghi F, Jimenez Diaz JF, Sande, R. EFSUMB Clinical Safety Statement for Diagnostic Ultrasound - (2019 revision). Ultraschall Med 2019. DOI: 10.1055/a-1010-6018

Liu YB, Herman BA, Soneson JE, Harris GR. Thermal safety simulations of transient temperature rise during acoustic radiation force-based ultrasound elastography. Ultrasound Med Biol 2014;40:1001–4.

Martin E, Shaw A, Lees C. Survey of current practice in clinical transvaginal ultrasound scanning in the UK. Ultrasound 2015;23:138–48.

Massó P, Rus G, Molina FS. Safety of elastography in fetal medicine: preliminary study on hypoacusis. Ultrasound Obst Gyn 2017;50:660–1.

Menten R, Leonard A, Clapuyt P, Vincke P, Nicolae A-C, Lebecque P. Transient elastography in patients with cystic fibrosis. Pediatr Radiol 2010;40:1231–5.

Metin MR, Aydın H, Ünal Ö, Akçay Y, Duymuş M, Türkyılmaz E, Avcu S. Differentiation between endometrial carcinoma and atypical endometrial hyperplasia with transvaginal sonographic elastography. Ultrasound Obst Gyn 2016;97:425–31.

Miloro P, Martin E, Shaw A. Temperature elevation measured in a tissue-mimicking phantom for transvaginal ultrasound at clinical settings. Ultrasound 2017;25:6–15.

Monpeyssen H, Tramalloni J, Poirée S, Hélénon O, Correas J-M. Elastography of the thyroid. Diagn Interv Radiol 2013;94:535–44.

Mottet N, Metz J-P, Chaussy Y. Evolution of fetal lung stiffness during gestation in two different congenital malformations. J Obstet Gynaecol Re 2019;45:931–4.

Nitta N, Ishiguro Y, Sasanuma H, Taniguchi N, Akiyama I. Experimental system for in-situ measurement of temperature rise in animal tissue under exposure to acoustic radiation force impulse. J Med Ultrason 2015;42:39–46.

Ogawa M, Nagao D, Mori K, Sato M, Sato A, Shimizu D, Terada Y. Elastography for differentiation of subchorionic hematoma and placenta previa. Ultrasound Obst Gyn 2012;39:112–4.

Ophir J, Céspedes I, Ponnekanti H, Yazdi Y, Li X. Elastography: a quantitative method for imaging the elasticity of biological tissues. Ultrasonic Imaging 1991;13:111–34.

Parker KJ, Doyley MM, Rubens DJ. Imaging the elastic properties of tissue: the 20 year perspective. Phys Med Biol. 2011;56:1–29.

Peralta L, Molina FS, Melchor J, Gómez LF, Massó P, Florido J, Rus G. Transient Elastography to Assess the Cervical Ripening during Pregnancy: A Preliminary Study. Ultraschall Med 2017;38:395–402.

449 Palmeri ML, Nightingale KR. On the thermal effects associated with radiation force imaging
450 of soft tissue. IEEE Trans Ultrason Ferroelectr Freq Control 2004;51:551–65.
451 Pereira S, Frick AP, Poon LC, Zamprakou A, Nicolaides KH. Successful induction of labor:
452 prediction by preinduction cervical length, angle of progression and cervical
453 elastography. Ultrasound Obst Gyn 2014;44:468–75.
454 Săftoiu A, Gilja OH, Sidhu PS, Dietrich CF, Cantisani V, Amy D, Bachmann-Nielsen M, Bob
455 F, Bojunga J, Brock M, Calliada F, Clevert DA, Correas JM, D'Onofrio M, Ewertsen C,
456 Farrokh A, Fodor D, Fusaroli P, Havre RF, Hocke M, Ignee A, Jenssen C, Klauser AS,
457 Kollmann C, Radzina M, Ramnarine KV, Sconfienza LM, Solomon C, Sporea I,
458 Stefanescu H, Tanter M, Vilmann P. The EFSUMB Guidelines and Recommendations
459 for the Clinical Practice of Elastography in Non-Hepatic Applications: Update 2018.
460 Ultraschall Med 2019;40:425–53.
461 Sandulescu L, Padureanu V, Dumitrescu C, Braia N, Streba CT, Gheonea DI, Cazacu S,
462 Ciurea T, Rogoveanu I, Saftoiu A. A Pilot Study of Real Time Elastography in the
463 Differentiation of Focal Liver Lesions. Curr Health Sci J 2012;38 :32–5.
464 Shankar H, Pagel PS. Potential Adverse Ultrasound-related Biological Effects A Critical
465 Review. Anesthesiology 2011;115:1109–24.
466 Shiina T, Nightingale KR, Palmeri ML, Hall TJ, Bamber JC, Barr RG, Castera L, Choi BI,
467 Chou YH, Cosgrove D, Dietrich CF, Ding H, Amy D, Farrokh A, Ferraioli G, Filice C,
468 Friedrich-Rust M, Nakashima K, Schafer F, Sporea I, Suzuki S, Wilson S, Kudo M.
469 WFUMB Guidelines and Recommendations for Clinical Use of Ultrasound Elastography:
470 Part 1: Basic Principles and Terminology. Ultrasound Med Biol 2015;41(5):1126–47.
471 Skurczynski MJ, Duck FA, Shipley JA, Bamber JC, Melodelima D. Evaluation of
472 experimental methods for assessing safety for ultrasound radiation force elastography. Br
473 J Radiol 2009;82:666–74.
474 Sugitani M, Fujita Y, Yumoto Y, Fukushima K, Takeuchi T, Shimokawa M, Kato K. A new
475 method for measurement of placental elasticity: acoustic radiation force impulse imaging.
476 Placenta 2013;34:1009–13.
477 Suo D, Clark A, Bonilla S, Keller S, Averkiou M. Controlled Bubble-Enhanced Heating With
478 Added Microbubbles. 19th Internarional Symposium of ISTU, Barcelona, Spain, 2019,
479 13th–15th June, p. 96.
480 Stoelinga B, Hehenkamp WJK, Brölmann H a. M, Huirne J a. F. Real-time elastography for
481 assessment of uterine disorders. Ultrasound Obst Gyn 2014;43:218–26.

Tabaru M, Yoshikawa H, Azuma T, Asami R, Hashiba K. Experimental study on temperature rise of acoustic radiation force elastography. J Med Ultrason 2012;39:137–46.

Wilson LS, Robinson DE. Ultrasonic measurement of small displacements and deformations of tissues. Ultrasonic Imaging 1982;4:71–82.

Zheng X-Z, Wu J, Tan X-Y. A novel approach to assessing fetal tissue stiffness using virtual touch tissue quantification. Med Ultrason 2016;18:70–4.

Figure Captions List

Figure 1. 3D-printed frame showing thermocouple placement: a) CAD drawing of the frame showing notches used to control horizontal thermocouple placement; b) photograph of the frame; c) front view of the frame with mounted thermocouples. The front and side walls of the frame were removed in the photographs; d) schematic view of the thermocouple locations (labelled 1 to 10 and ref) and definition of the x, y, z axis directions; e) same in top view, with imaging plane highlighted.

Figure 2. a) Picture of the experimental setup showing the clamp arrangement used to hold the imaging probe in a static position; b) B-mode image of the phantom showing thermocouple wires.

Figure 3. Temperature change of the ten thermocouples as a function of time: a) for B-mode; b) for PD; c) for SWE. For a better visualization of the lowest thermal responses, temperature changes at 400 s can be seen in Fig. 4.

Figure 4. Temperature change for the three tested ultrasound imaging modes at 400 s (corresponding to the end of the 380 s exposure duration). For each mode, the circle diameter is proportional to the temperature change with the diameter for Tc-1 (maximum temperature change) being set to be the same (normalized) for the three modes in order to reveal relative temperature distributions within each mode.

Figure 5. Comparison of temperature changes for B-mode, PD and SWE imaging exposures for thermocouple: a) Tc-1, b) Tc-10*, c) Tc-7.

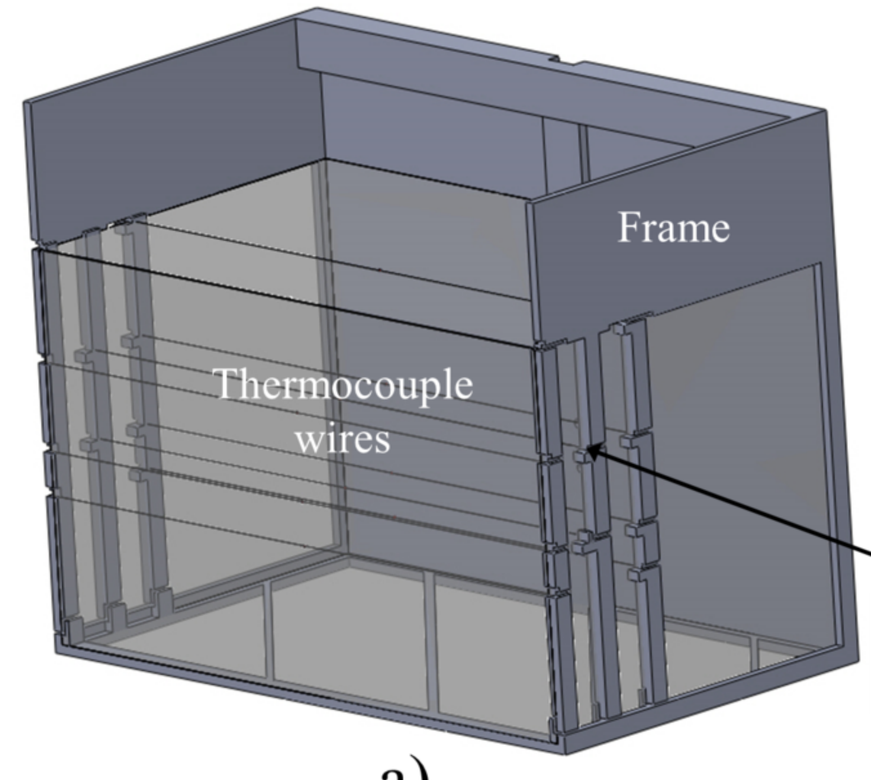
Frame
Thermocouple wires

a)

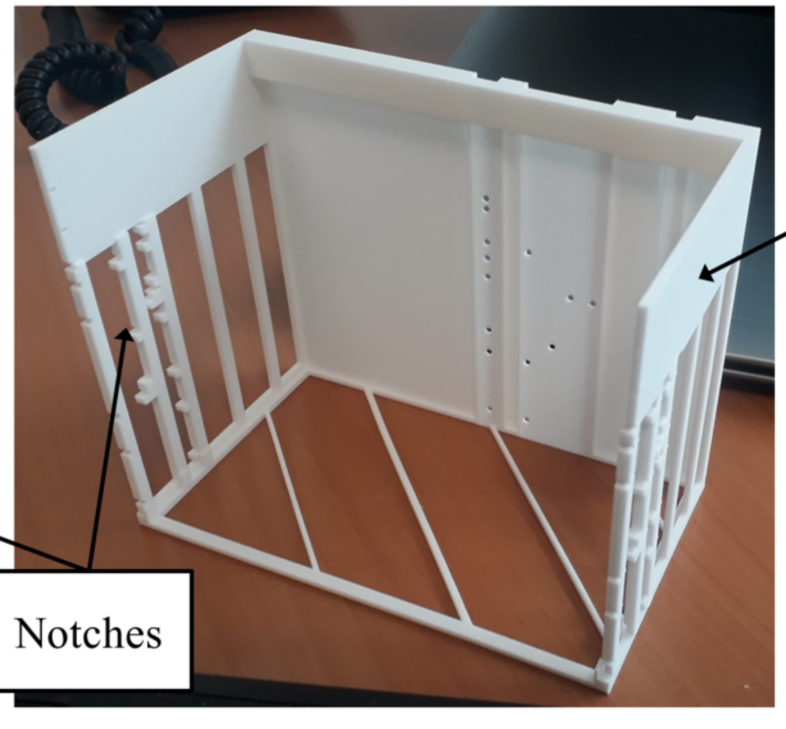
Notches

b)

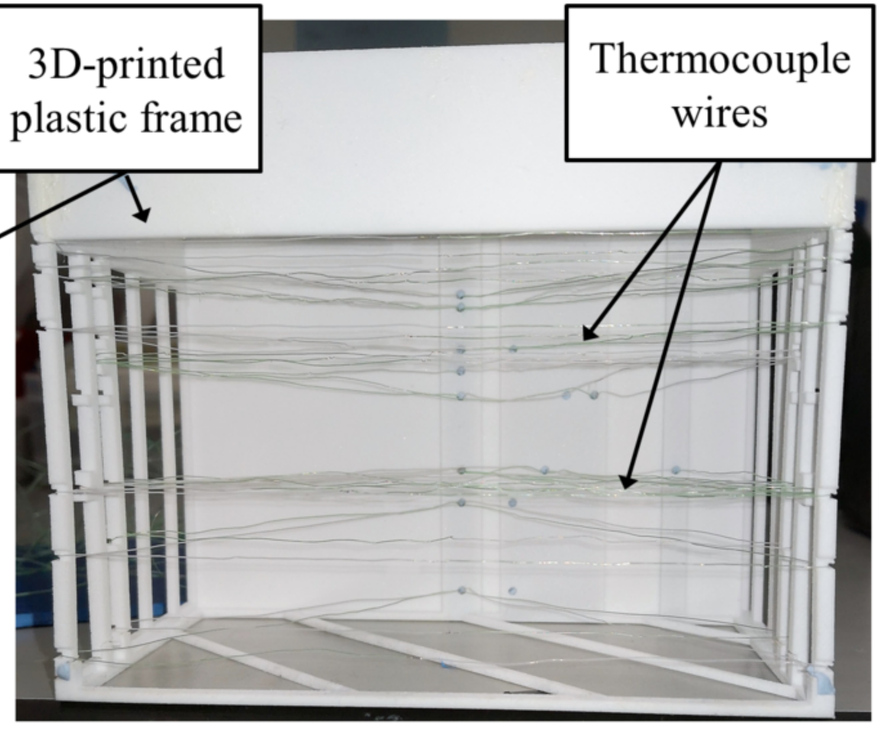
3D-printed plastic frame
Thermocouple wires

c)

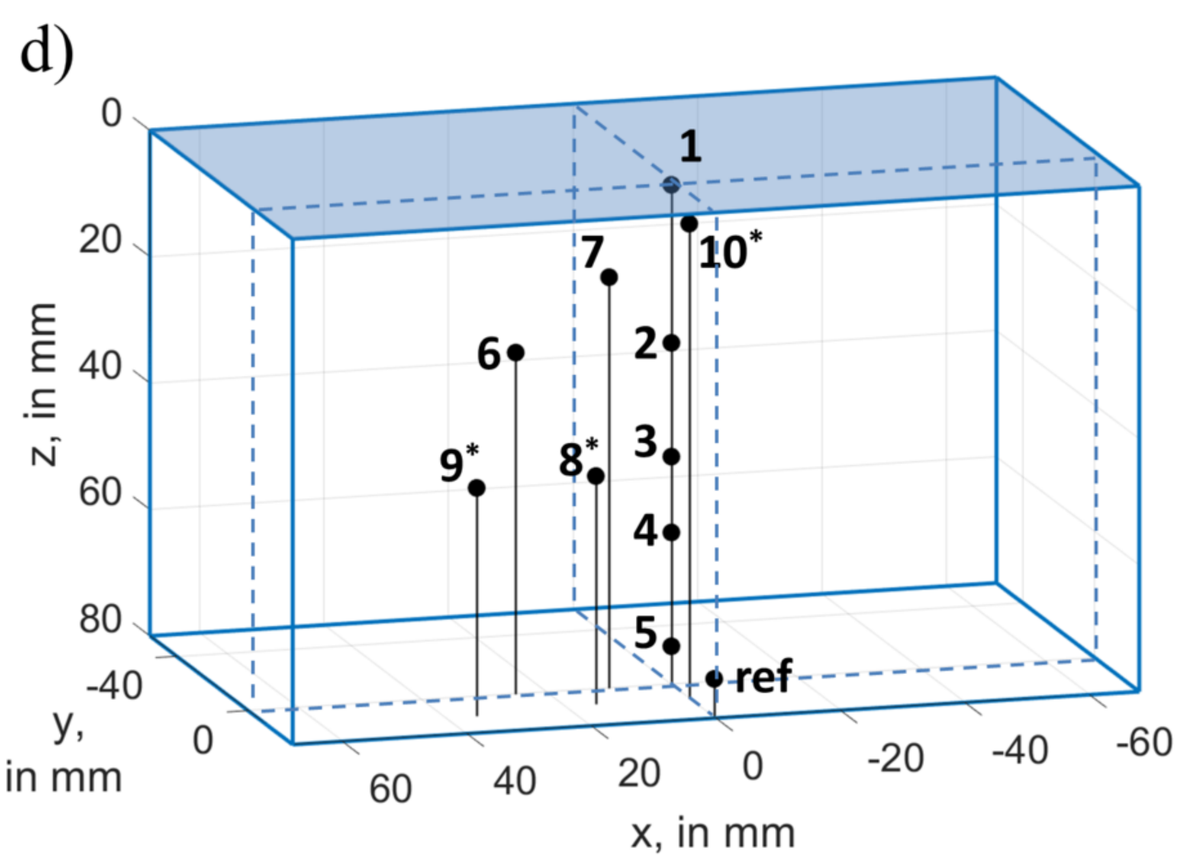
d)
1
2
3
4
5
6
7
8*
9*
10*
ref
z, in mm
y, in mm
x, in mm

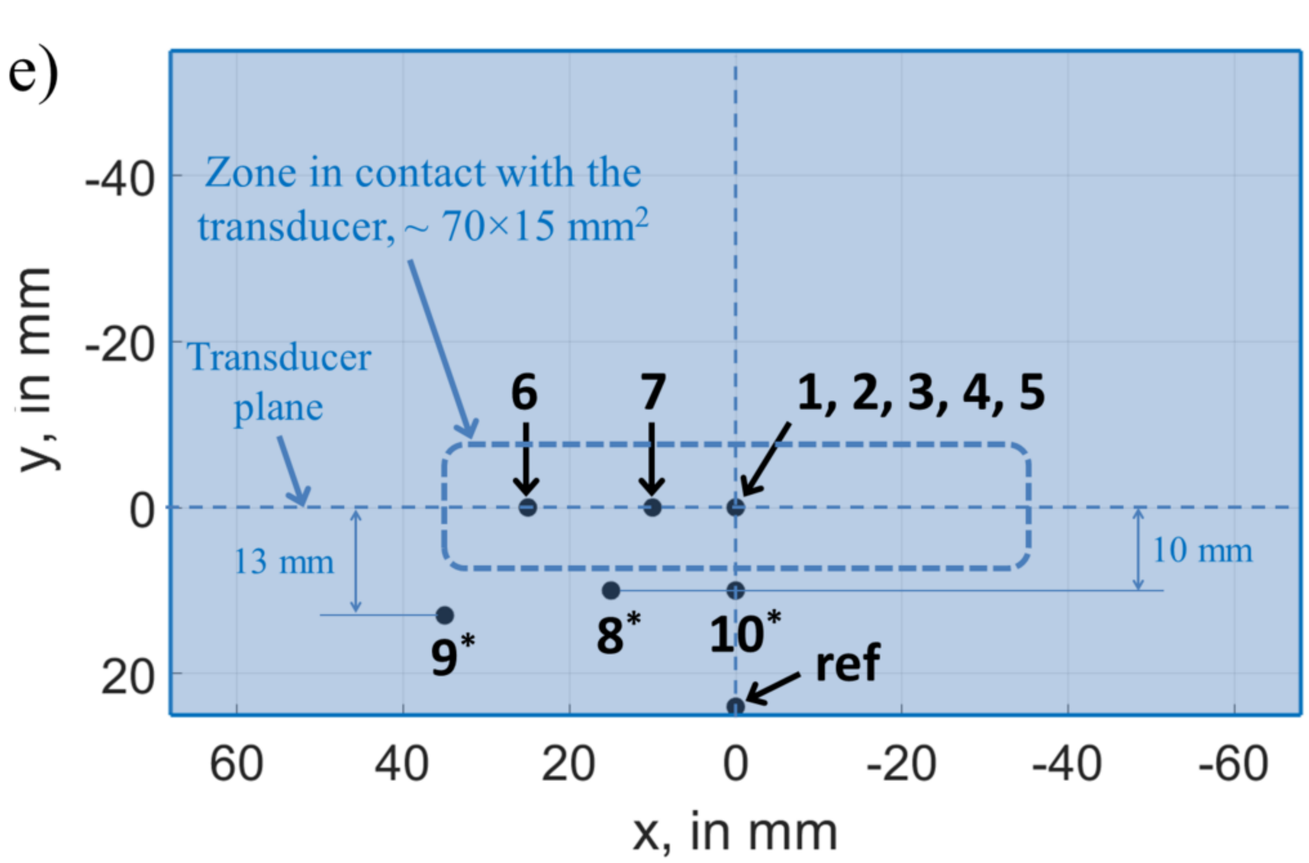
e)
Zone in contact with the transducer, ~ 70×15 mm²
Transducer plane
6
7
1, 2, 3, 4, 5
13 mm
10 mm
9*
8*
10*
ref
y, in mm
x, in mm

a)

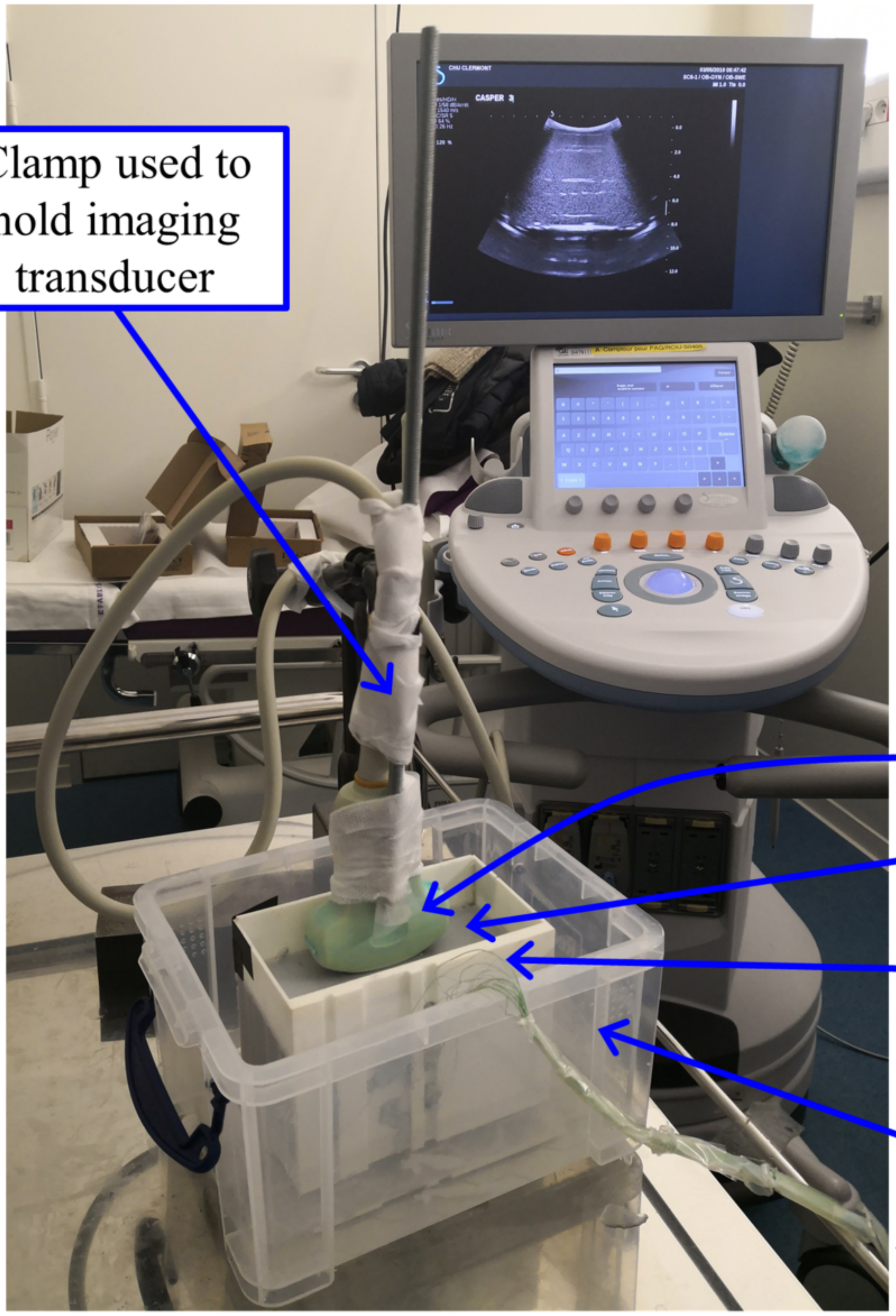
Clamp used to hold imaging transducer
Aixplorer® scanner
Transducer
Phantom
3D-printed frame
Plastic box containing ~ 2 cm of glycerol
Thermocouple output

b)

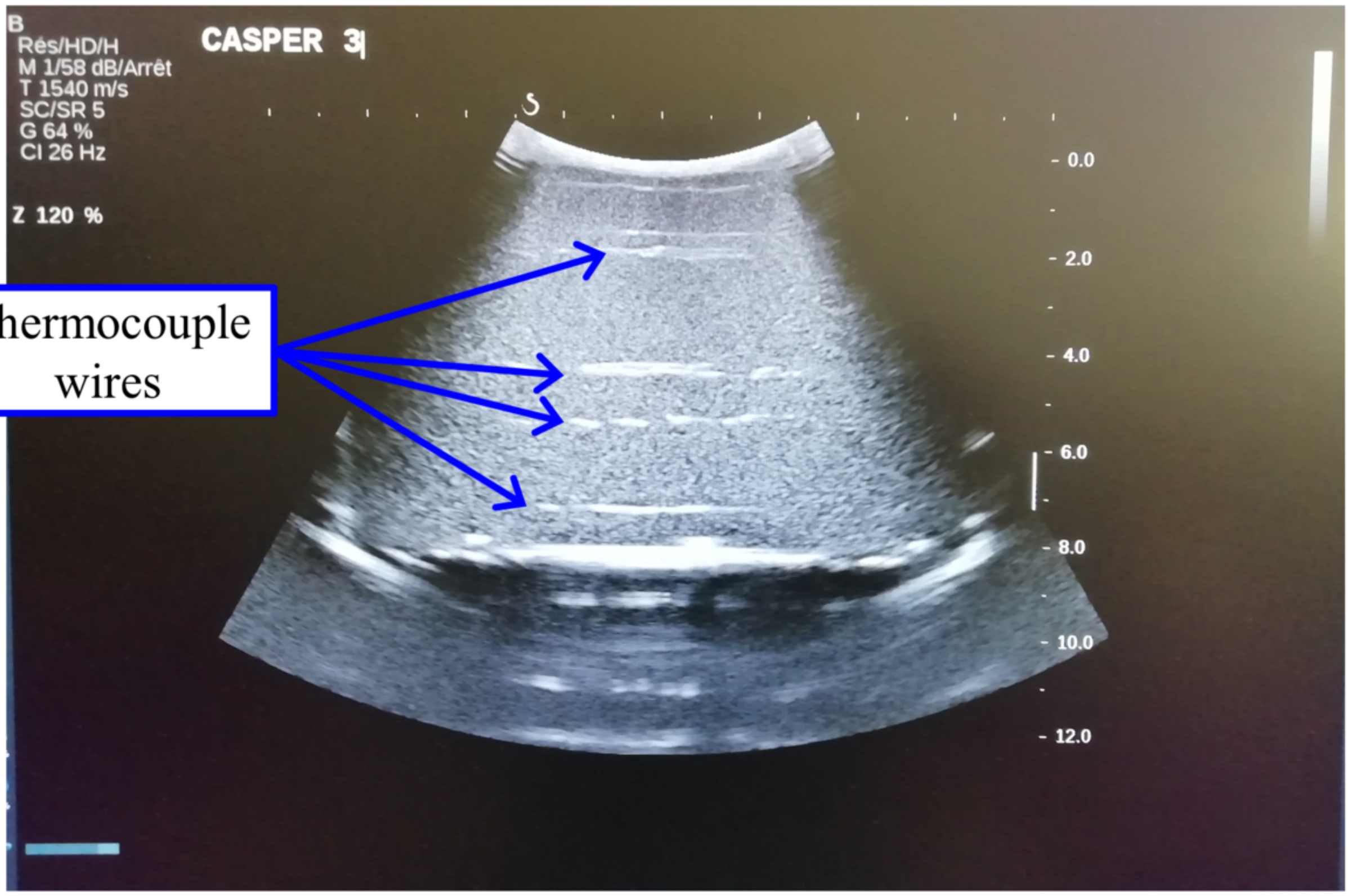
B
Rés/HD/H
M 1/58 dB/Arrêt
T 1540 m/s
SC/SR 5
G 64 %
CI 26 Hz
Z 120 %
CASPER 3
0.0
2.0
4.0
6.0
8.0
10.0
12.0
Thermocouple wires

a)

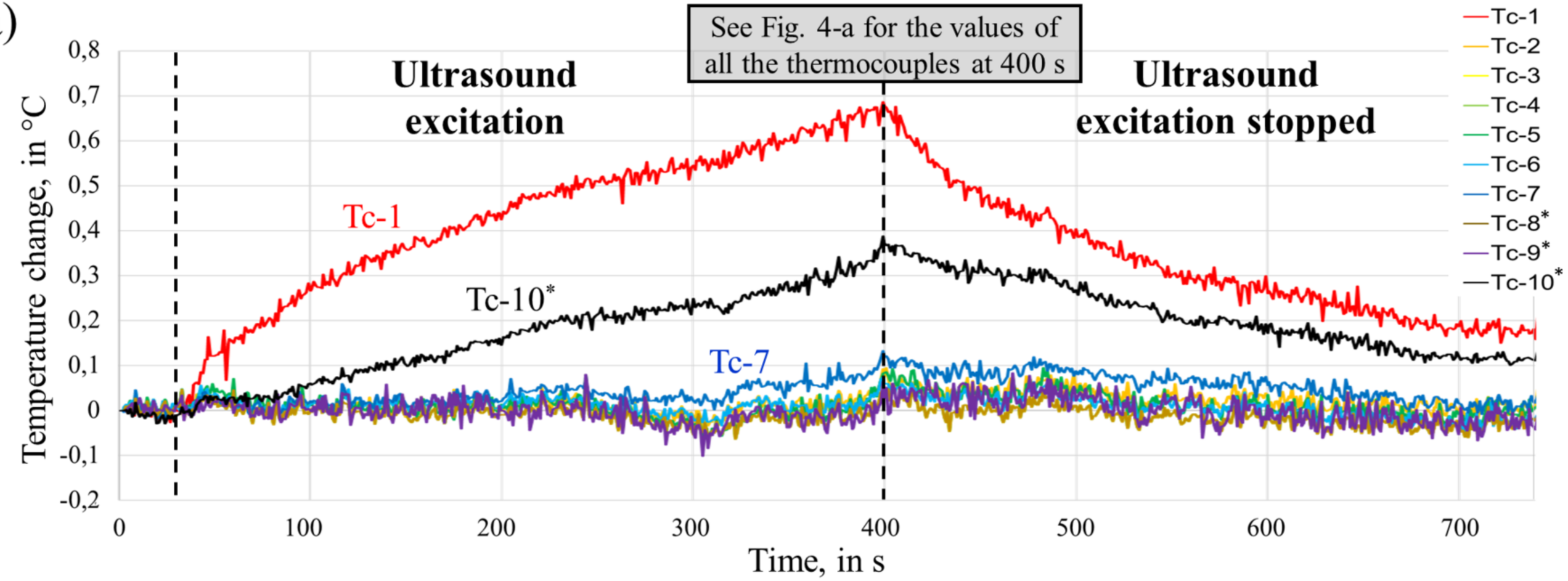
See Fig. 4-a for the values of all the thermocouples at 400 s
Ultrasound excitation
Ultrasound excitation stopped
Tc-1
Tc-10*
Tc-7
Temperature change, in °C
Time, in s
0,8
0,7
0,6
0,5
0,4
0,3
0,2
0,1
0
-0,1
-0,2
0
100
200
300
400
500
600
700
Tc-1
Tc-2
Tc-3
Tc-4
Tc-5
Tc-6
Tc-7
Tc-8*
Tc-9*
Tc-10*

b)

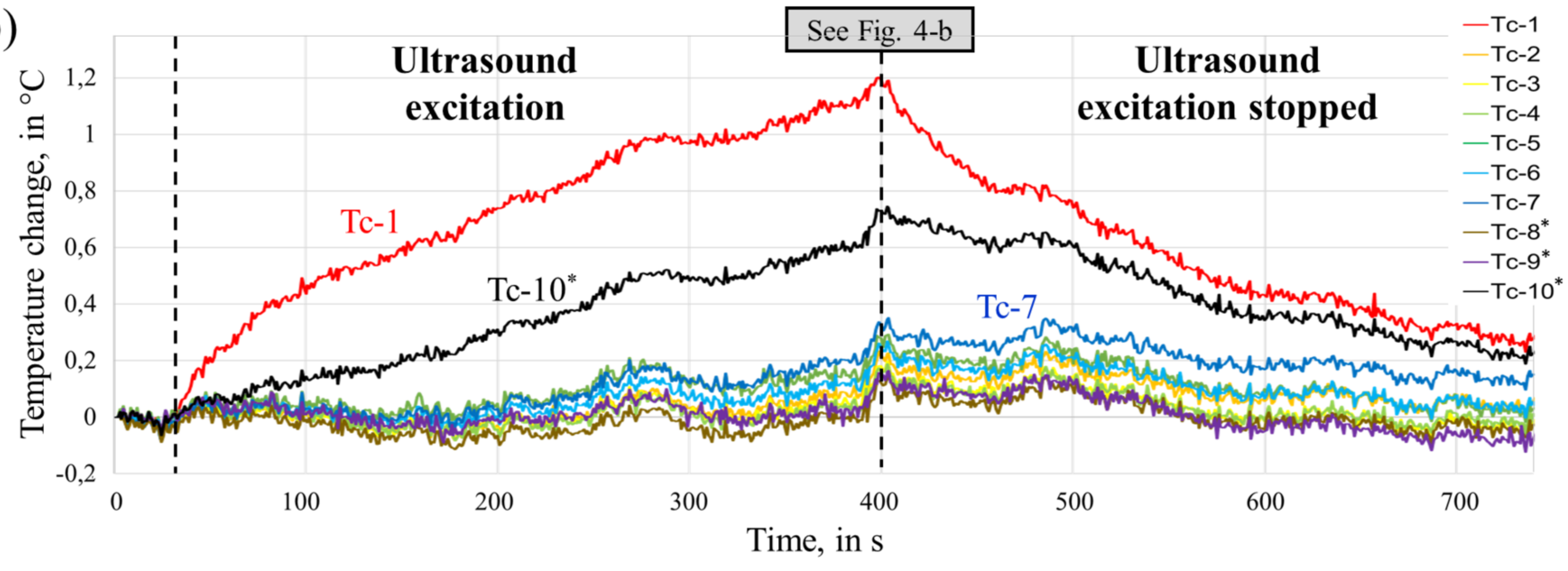
See Fig. 4-b
Ultrasound excitation
Ultrasound excitation stopped
Tc-1
Tc-10*
Tc-7
Temperature change, in °C
Time, in s
1,2
1
0,8
0,6
0,4
0,2
0
-0,2
0
100
200
300
400
500
600
700
Tc-1
Tc-2
Tc-3
Tc-4
Tc-5
Tc-6
Tc-7
Tc-8*
Tc-9*
Tc-10*

c)

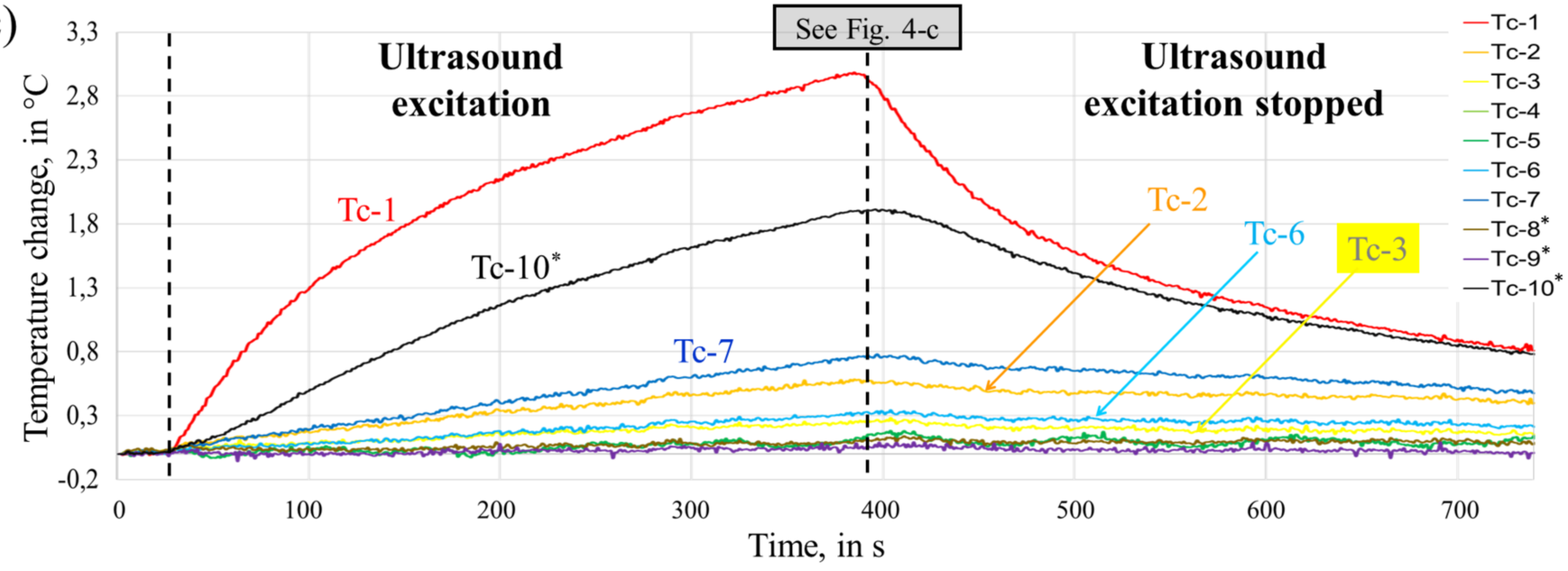
See Fig. 4-c
Ultrasound excitation
Ultrasound excitation stopped
Tc-1
Tc-10*
Tc-7
Tc-2
Tc-6
Tc-3
Temperature change, in °C
Time, in s
3,3
2,8
2,3
1,8
1,3
0,8
0,3
-0,2
0
100
200
300
400
500
600
700
Tc-1
Tc-2
Tc-3
Tc-4
Tc-5
Tc-6
Tc-7
Tc-8*
Tc-9*
Tc-10*

a)

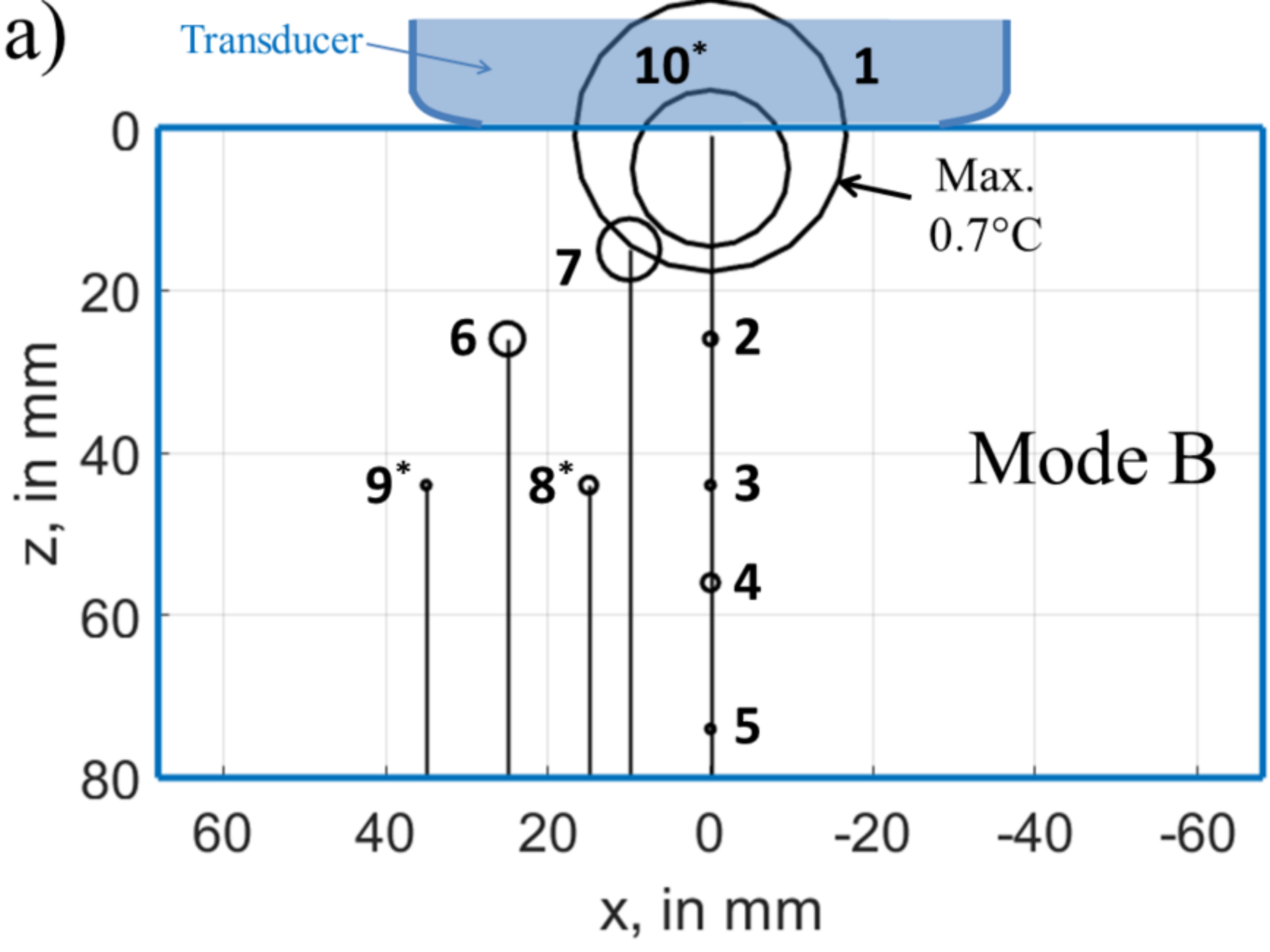
Transducer
10*
1
Max.
0.7°C
7
6
2
9*
8*
3
4
5
Mode B
z, in mm
0
20
40
60
80
60
40
20
0
-20
-40
-60
x, in mm

b)

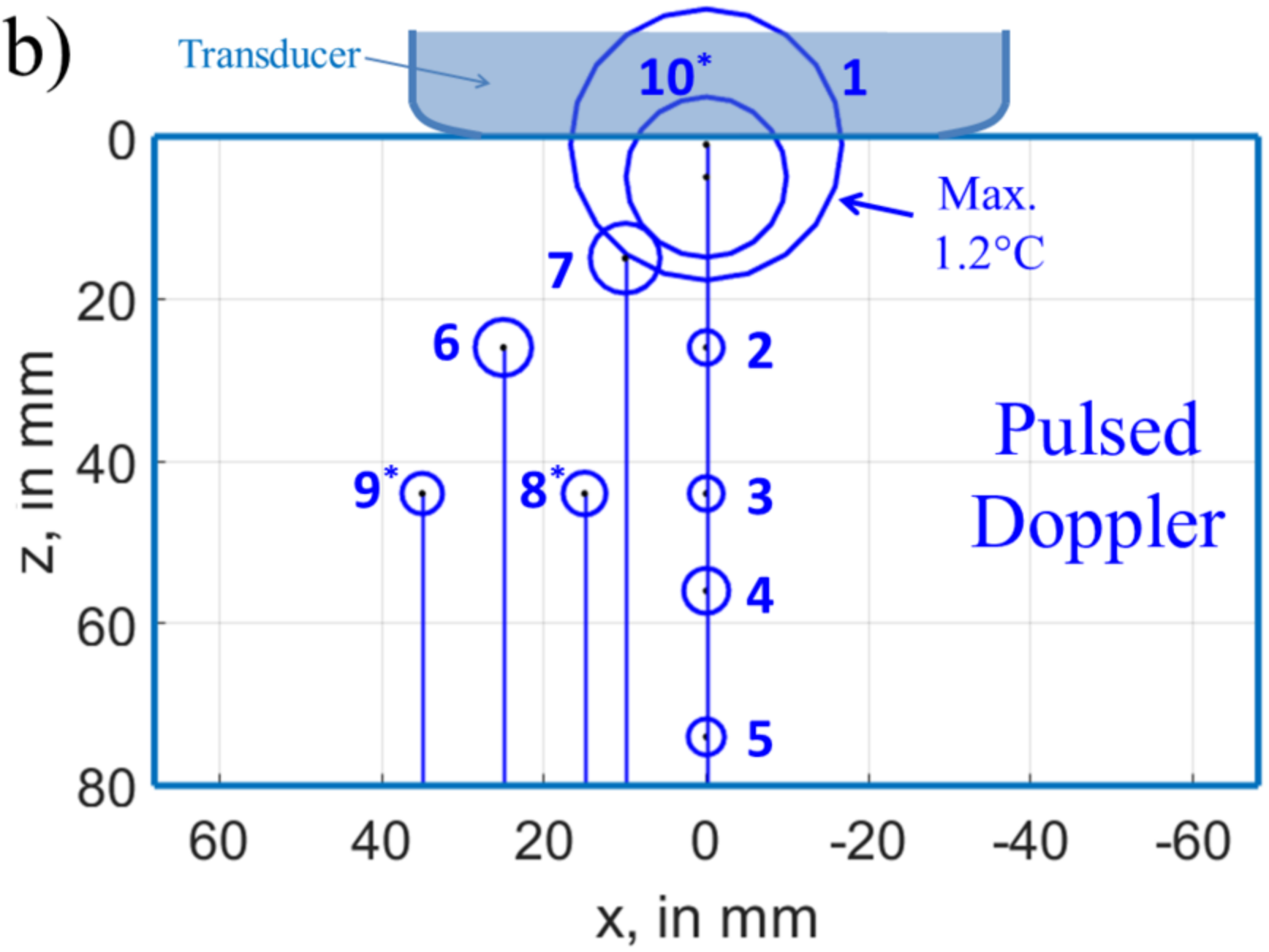
Transducer
10*
1
Max.
1.2°C
7
6
2
9*
8*
3
4
5
Pulsed
Doppler
z, in mm
0
20
40
60
80
60
40
20
0
-20
-40
-60
x, in mm

c)

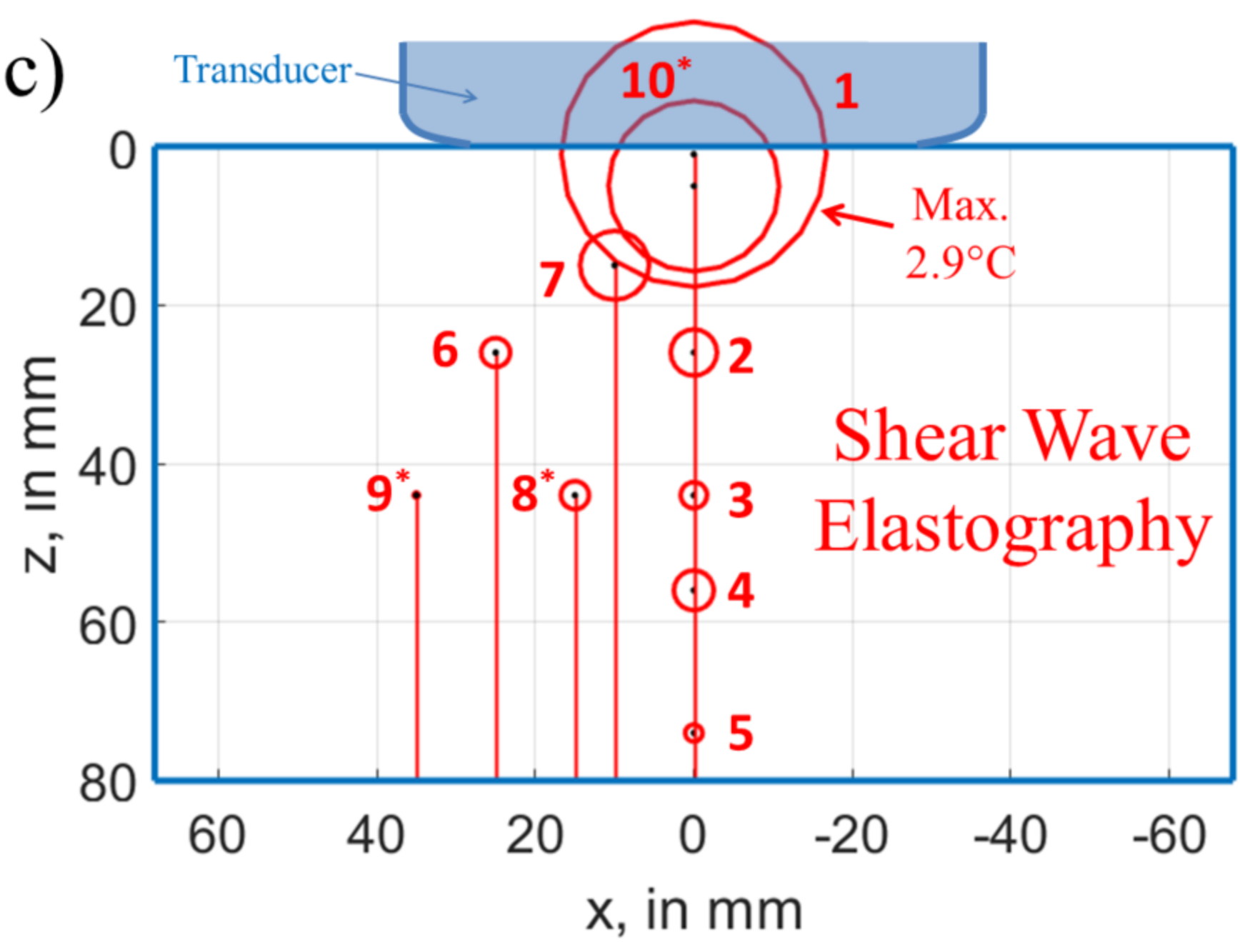
Transducer
10*
1
Max.
2.9°C
7
6
2
9*
8*
3
4
5
Shear Wave
Elastography
z, in mm
0
20
40
60
80
60
40
20
0
-20
-40
-60
x, in mm

a)

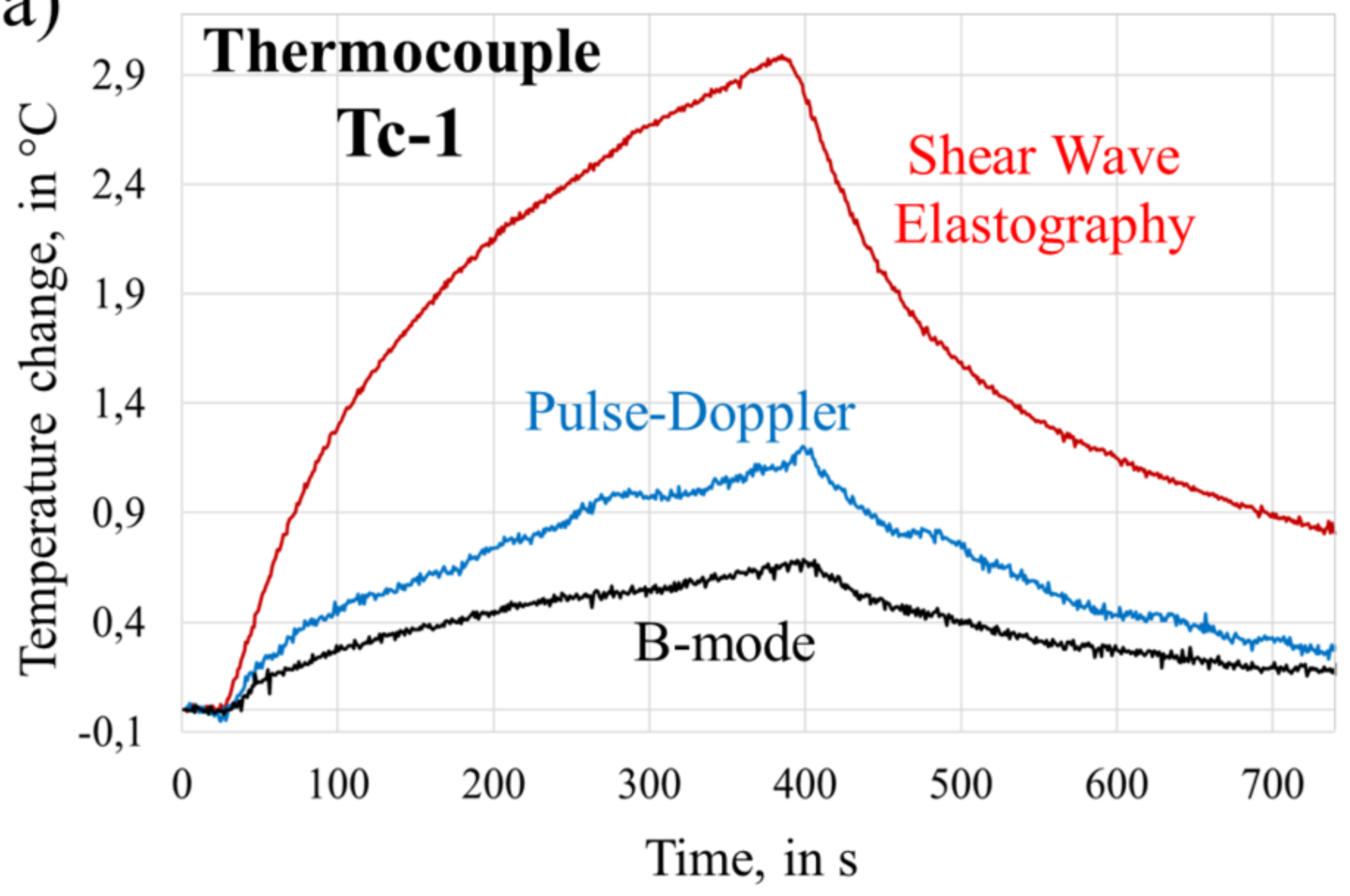
Thermocouple
Tc-1
Shear Wave
Elastography
Pulse-Doppler
B-mode
Temperature change, in °C
2,9
2,4
1,9
1,4
0,9
0,4
-0,1
0
100
200
300
400
500
600
700
Time, in s

b)

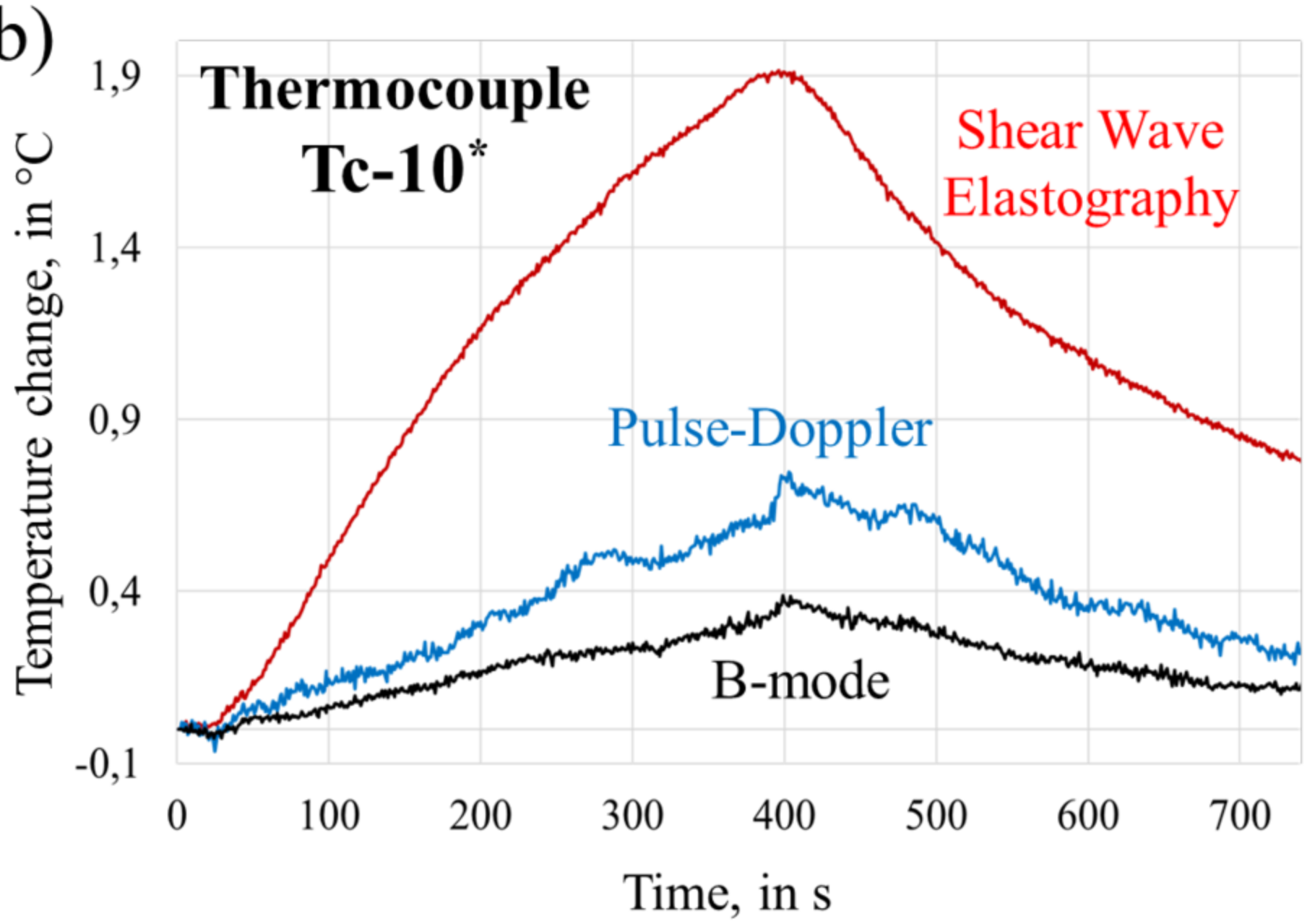
Thermocouple
Tc-10*
Shear Wave
Elastography
Pulse-Doppler
B-mode
Temperature change, in °C
1,9
1,4
0,9
0,4
-0,1
0
100
200
300
400
500
600
700
Time, in s

c)

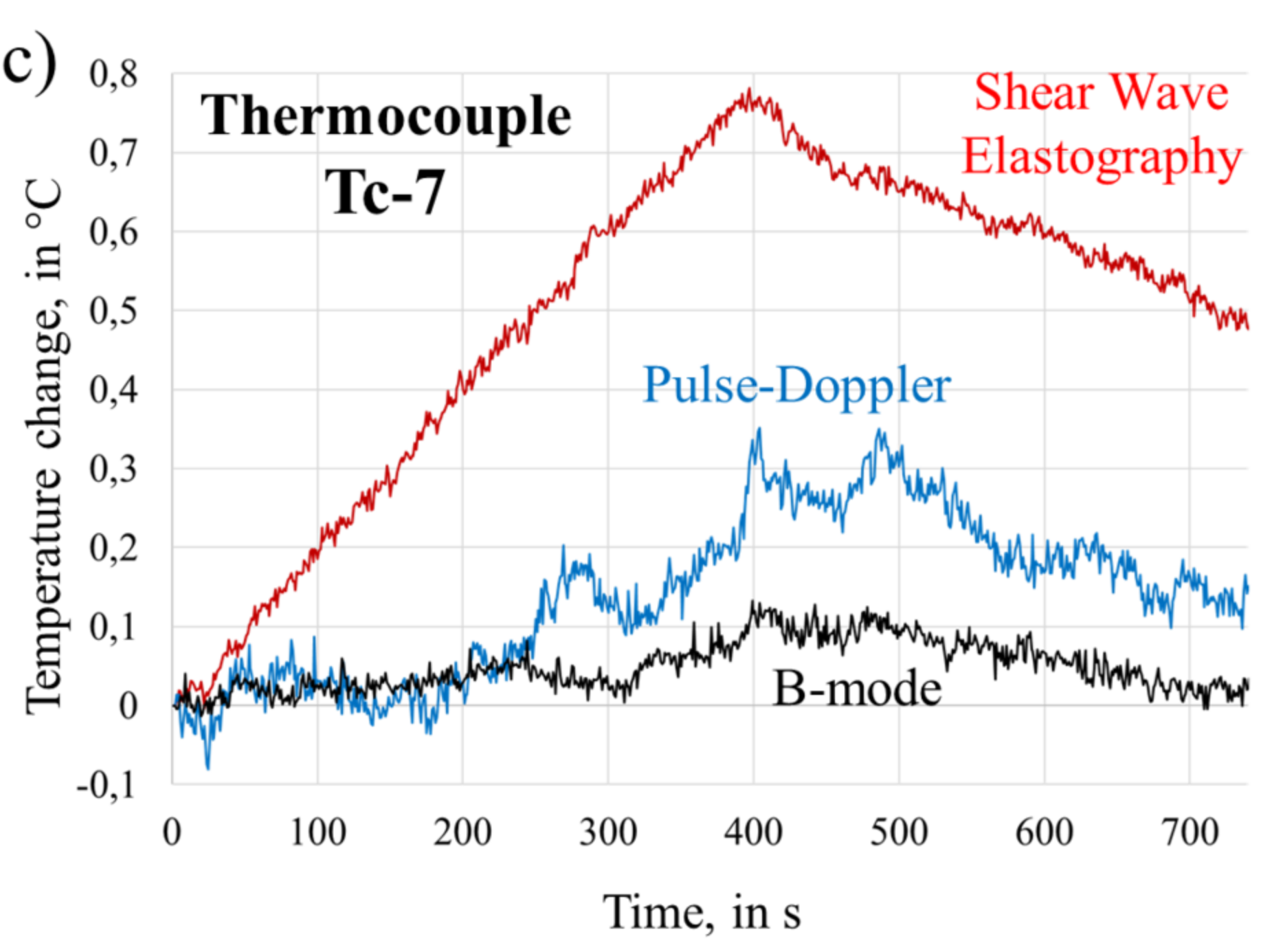
Thermocouple
Tc-7
Shear Wave
Elastography
Pulse-Doppler
B-mode
Temperature change, in °C
0,8
0,7
0,6
0,5
0,4
0,3
0,2
0,1
0
-0,1
0
100
200
300
400
500
600
700
Time, in s

Table 1. Coordinates (in mm) of the ten thermocouples used to track the temperature change due to ultrasound excitation. The origin of the coordinates system is shown in Fig. 1-d. An asterisk is used to specify the thermocouples located beyond the imaging plane (which is at $y = 0$ mm).

	Tc-1	Tc-2	Tc-3	Tc-4	Tc-5	Tc-6	Tc-7	Tc-8*	Tc-9*	Tc-10*
x	0	0	0	0	0	25	10	15	35	0
y	0	0	0	0	0	0	0	10	13	10
z	1	26	44	56	74	26	15	44	44	5

Table 2. Scanner settings for the three ultrasound modes used: B-mode, Pulse-Doppler (PD) and Shear Wave Elastography (SWE).

Parameters (OB-GYN GenOB preset)	**B-mode**	**PD**	**SWE**
Total depth	80 mm	22 mm	80 mm
B-mode focal zone	10 – 40 mm	22 mm	25 – 40 mm
Tissuetuner (Speed of sound used to transmit and receive beamforming)	1540 m/s	1540 m/s	1540 m/s
SWE Opt (Res, Std, Pen) for the optimization of elastography resolution and penetration	N/A	N/A	Standard
SWE box geometry	N/A	N/A	Top width: 43.9 mm Bottom width: 63.2 mm Height: 30.8 mm Top depth: 6.7 mm
MI (Mechanical Index)	1.2	1	1.5
TIb (Thermal Index bone)	0	0	1.6
TIs (Thermal Index soft tissue)	0	0	1.4